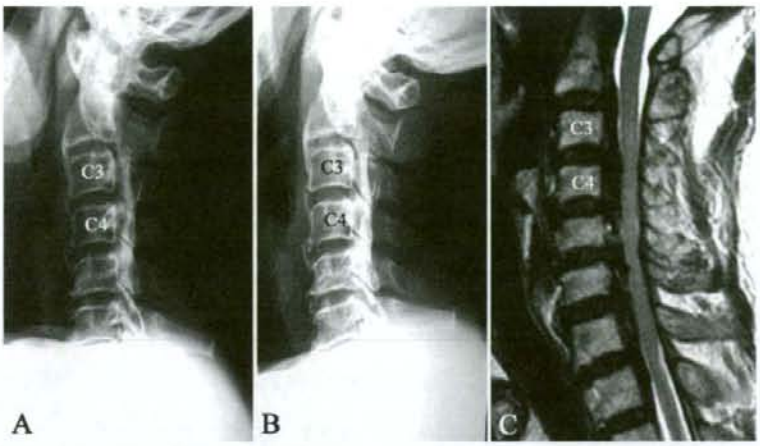

FIG. 2. Case 1. Flexion (A) and extension (B) cervical radiographs obtained at presentation in a patient with mixed-type OPLL. The residual space available for the cord is 7 mm at C3–4, and the C1–7 ROM is 23°. Anterior impingement of the spinal cord at several levels is visible on a T2-weighted, midsagittal MR image (C), but no HSCs are visible.

(range 25–63%) in the conservative group and 40% (range 25–61%) in the surgical group. The residual space available for the cord was 7.9 mm (range 6–11 mm) in the conservative group and 9.3 mm (range 6–12 mm) in the surgical group. No significant differences were seen on imaging data between the 2 groups.

The mean ROM at C1–7 at the initial consultation was 36.4° (range 15–62°) in the conservative treatment group and 46.5° (range 26–64°) in the surgical group. The mobility of the spinal column between C-1 and C-7 was therefore significantly greater in the surgical group ($p < 0.05$). Nineteen of 20 patients in the surgical group had a C1–7 ROM ≥ 35°, whereas 11 of 21 patients in the conservative treatment group had a C1–7 ROM ≥ 35° ($p < 0.05$). The C1–7 ROM in the conservative group was measured until the most recent follow-up. The mean C1–7 ROM at the final follow-up examination was 33° (range 11–50°) in the conservative group, indicating that no significant changes had occurred since the initial consultation.

High signal changes on T2-weighted images were not seen in any patient in the conservative treatment group, whereas 17 patients in the surgical group had HSCs. Thus, the incidence of HSCs in the spinal cord was significantly higher among patients in the surgically treated group than in the conservative group ($p < 0.05$). During the follow-up period, no HSCs developed in the conservative group.

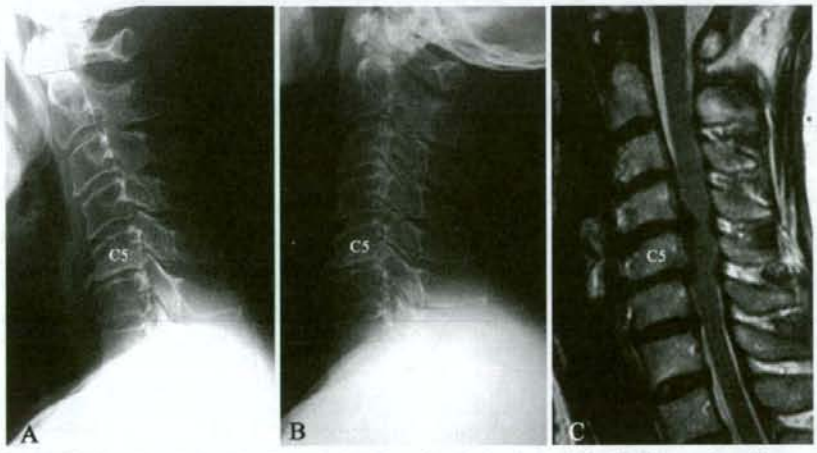

FIG. 3. Case 2. Flexion (A) and extension (B) cervical radiographs obtained at the initial visit in a patient with segmental-type OPLL. The residual space available for the cord is 9 mm at the C-5 level, and the C1–7 ROM is 52°. A T2-weighted midsagittal MR image obtained at presentation (C) indicates that impingement of the spinal cord at the C4–5 level is seen, but no HSCs are visible.

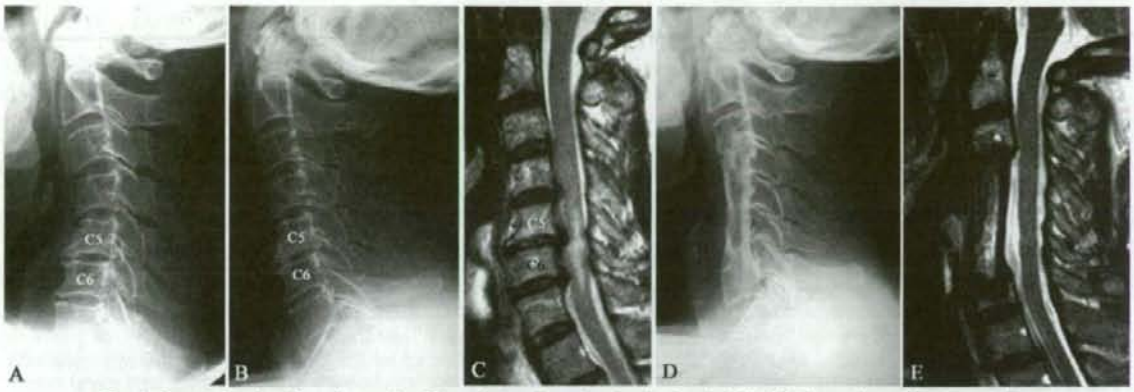

FIG. 4. Case 3. Flexion (A) and extension (B) cervical radiographs obtained at the initial visit in a patient with segmental-type OPLL. The residual space available for the cord was 10 mm at the C5–6 level, and the C1–7 ROM was 57°. A T2-weighted midsagittal MR image (C) obtained at presentation shows impingement on the spinal cord at multiple levels in both the anterior and posterior directions, and HSCs are evident in the spinal cord, especially at C5–6 and C6–7. Lateral cervical radiograph (D) obtained 2 years after surgery shows successful spinal fusion with fibula autograft. A T2-weighted midsagittal MR image obtained 1 year postoperatively (E) shows decompression and diminished cord HSCs.

Illustrative Cases

Case 1: Patient in the Conservative Treatment Group Without Improvement

This 68-year-old man with mixed-type OPLL complained of neck stiffness for 20 years and was recommended for surgery. At the initial examination, he showed no sign of myelopathy and he had a JOA score of 17. A lateral cervical radiograph obtained at the first visit showed that the DSSD was 16 mm, % ratio was 56%, and the residual space available for the cord was 7 mm at the C3–4 level. Flexion and extension radiography revealed that the C1–7 ROM was 23°, indicating a relatively small amount of spinal mobility (Fig. 2A and B). Midsagittal T2-weighted MR images showed no HSCs in the spinal cord, although obstruction of the subarachnoid space with anterior impingement of the spinal cord was found at several levels (Fig. 2C). The patient was followed up conservatively. During the follow-up period of 2 years, his neck stiffness persisted but no myelopathy developed.

Case 2: Patient in the Conservative Treatment Group With Clinical Worsening

This 59-year-old woman presented with complaints of mild numbness in all of her fingers and bilateral clumsiness of her hands caused by segmental OPLL at C-5. Deep tendon reflexes were hyperactive in her lower extremities, but she did not have any gait disturbance; her JOA scale score was 15.5. A lateral cervical radiograph obtained at the first visit showed that the DSSD was 14.5 mm, % ratio was 38%, and residual space available for the cord was 9 mm at the C-5 level. Flexion and extension radiographs showed that the C1–7 ROM was 52°, indicating an extensive degree of spinal mobility (Fig. 3A and B). Midsagittal T2-weighted MR images showed impingement of the spinal cord at the C4–5 level from both the anterior and posterior directions due to a thickened posterior longitudinal ligament and ligamentum flavum, but no signal change was seen in the spinal cord at this level (Fig. 3C). Over a 3-year follow-up period, the patient complained of increasing numbness and clumsiness, with a decreased JOA scale score of 14.5 points.

Case 3: Patient in the Surgical Treatment Group

This 58-year-old man presented with bilateral upper arm weakness and gait disturbance. A lateral cervical radiograph obtained at the first visit showed segmental type OPLL (C-4, C-5, C-6, and C-7) with a DSSD of 16 mm, % ratio of 37.5%, and 10-mm residual space for the cord at the level of C5–6. Flexion and extension radiographs demonstrated that the C1–7 ROM was 57°, an extensive degree of spinal mobility (Fig. 4A and B). Impingement of the spinal cord at multiple levels from both the anterior and posterior directions was shown on T2-weighted midsagittal MR imaging, and HSCs were evident in the spinal cord, especially at the C5–6 and C6–7 levels (Fig. 4C). The patient's preoperative JOA scale score was 11.5 points. He underwent anterior excision of OPLL and spinal fusion with fibula autograft. Postoperatively, the patient improved neurologically. Cervical radiographs obtained 2 years later revealed that spinal fusion was accomplished (Fig. 4D). Midsagittal T2-weighted MR images obtained 1 year postsurgery showed that the spinal cord was decompressed and the HSCs in the cord were diminished (Fig. 4E). At the final follow-up examination 3 years after surgery, the patient's JOA scale score was 16 points (recovery rate 81.8%).

Discussion

In the present study, we assigned patients with cervical OPLL to treatment groups based on myelopathy se-

verity and investigated the clinical course in patients with no or mild myelopathy despite the presence of OPLL-induced spinal canal narrowing. Of 21 patients with no or only mild myelopathy, newly developed myelopathy was not seen in any patient, and slight aggravation of preexisting myelopathy occurred in only 1 patient (4.8%). Thus, clinical symptoms were unchanged or improved in 95.2% of patients, although they had OPLL-induced spinal canal narrowing with ≤ 12 mm of residual space available for the spinal cord. These results suggest that our criterion for conservative treatment (a JOA scale score ≥ 14 points) is appropriate. On the basis of our findings in the present study, we suggest that decompression surgery at an early stage is not recommended in most patients with OPLL who have no or mild myelopathy, even in the presence of OPLL-induced spinal canal narrowing.

Regarding factors that influence the development of myelopathy in patients with cervical OPLL, several reports have demonstrated the importance of static compression factors, which are expressed in % ratios and measurements of the residual space available for the spinal cord.[4,5,9,13] In younger patients, such static compression factors preferentially contribute to the development and aggravation of myelopathy because of the presence of strong growth activity of the ossified mass.[3] In addition to static compression factors, recent reports have described dynamic factors, such as spinal column mobility, in the development of myelopathy in patients with a considerable degree of OPPL canal occupation.[8,9,12]

In the present study, the mobility of the cervical spine, which was analyzed as the C1–7 ROM, participated in the development of myelopathy in patients with OPLL-induced spinal canal narrowing, but the % ratio and the residual space available for the cord did not. In addition, our results indicate the contribution of the morphological subtypes of OPLL to the development of myelopathy. Patients with segmental-type OPLL generally have increased mobility of the cervical spine compared with patients with continuous-type OPLL. We speculate that when OPLL-induced canal stenosis develops in patients with segmental-type OPLL, the relatively larger cervical mobility is maintained and myelopathy will be more likely to occur than in patients with continuous-type OPLL. In the majority of patients who suffered from moderate and severe myelopathy and who underwent surgery, the C1–7 ROMs were ≥ 35° at the initial consultation. We therefore suggest that having a C1–7 ROM of ≥ 35° is a risk factor for the development or aggravation of myelopathy in patients with OPLL-induced canal stenosis. In support of this hypothesis is the fact that the only patient in the conservative treatment group (Case 2) who experienced clinical deterioration during the follow-up period had a 52° ROM at C1–7.

Previous studies have shown that high signal intensity in the spinal cord in T2-weighted MR images may correlate with some spinal cord disorders including attenuated venous circulation.[1] In the present study, the incidence of the HSCs was significantly higher in patients with moderate and severe myelopathy who underwent surgery. We suggest that increased myelopathy is more likely to occur in patients with cervical OPLL and spinal canal narrowing who show high signal intensity on imaging at their initial presentation.

In view of our results and previous findings,[9,11,12] when we decide the treatment procedure for patients with OPLL-induced canal stenosis and no or mild myelopathy, conservative treatment is the first choice if 1) the C1–7 ROM is < 35°; 2) OPLL type is continuous; 3) the patient is older than 50 years of age; and 4) no HSCs are seen in the spinal cord on T2-weighted MR images. In contrast, surgical treatment is indicated if 1) the C1–7 ROM is ≥ 35°; 2) OPLL type is segmental; 3) the patient is younger than 50 years of age and has activated growth activity of the ossified mass; and 4) a high signal intensity is seen in the spinal cord and there is a risk of myelopathy or aggravation of existing myelopathy. When we undertake surgery in patients with cervical OPLL and canal stenosis, we consider not only the need for spinal cord decompression but also the suppression of dynamic factors. Thus, we believe that complete excision of the ossified mass using an anterior approach in combination with the stabilization of the spine column with strut bone graft is theoretically the best procedure.

To the best of our knowledge, ours is the first study to base treatment in patients with cervical OPLL on the severity of myelopathy and to investigate the natural clinical course in patients with cervical OPLL and no or mild myelopathy. Our findings provide guidance for deciding on the appropriate timing of surgery in patients with cervical OPLL who have significant cord compression caused by OPLL and early myelopathy. Nevertheless, our retrospective study design and relatively small number of patients should be considered when interpreting the results.

Conclusions

In the present study, we demonstrated that mobility of the cervical spine and morphological types of OPLL are important factors that can contribute to the development and aggravation of cervical myelopathy in patients with OPLL-induced canal stenosis. We advocate conservative treatment for most patients with OPLL and no or mild myelopathy, even in cases of spinal canal narrowing.

Disclosure

This work was supported by a Grant for Intractable Diseases from the Public Health Bureau, the Ministry of Health, Labour and Welfare of Japan (Investigation Committee on Ossification of the Spinal Ligaments).

References

1. Chen C, Lyu R, Wong Y, Wang L: Intramedullary high signal intensity on T2-weighted MR images in cervical spondylotic myelopathy: Prediction of prognosis with type of intensity. **Radiology 221:**789–794, 2001
2. Epstein N: Diagnosis and surgical management of cervical ossification of the posterior longitudinal ligament. **Spine J 2:**436–449, 2002
3. Hori T, Kawaguchi Y, Kimura T: How does the ossification area of the posterior longitudinal ligament thicken following cervical laminoplasty? **Spine 32:**E551–E556, 2007
4. Iwasaki M, Okuda S, Miyauchi A, Sakaura H, Mukai Y,

Yonenobu K, et al: Surgical strategy for cervical myelopathy due to ossification of the posterior longitudinal ligament: Part 1: clinical results and limitations of laminoplasty. **Spine 32:**647–653, 2007
5. Iwasaki M, Okuda S, Miyauchi A, Sakaura H, Mukai Y, Yonenobu K, et al: Surgical strategy for cervical myelopathy due to ossification of the posterior longitudinal ligament: Part 2: advantages of anterior decompression and fusion over laminoplasty. **Spine 32:**654–660, 2007
6. Masaki Y, Yamazaki M, Okawa A, Aramomi M, Hashimoto M, Koda M, et al: An analysis of factors causing poor surgical outcome in patients with cervical myelopathy due to ossification of the posterior longitudinal ligament: anterior decompression with spinal fusion versus laminoplasty. **J Spinal Disord Tech 20:**7–13, 2007
7. Matsumoto M, Toyama Y, Ishikawa M, Chiba K, Suzuki N, Fujimura Y: Increased signal intensity of the spinal cord on magnetic resonance images in cervical compressive myelopathy. **Spine 25:**677–682, 2000
8. Matsunaga S, Sakou T, Taketomi E, Yamaguchi M, Okano T: The natural course of myelopathy caused by ossification of the posterior longitudinal ligament in the cervical spine. **Clin Orthop Relat Res 305:**168–177, 1994
9. Matsunaga S, Kukita M, Hayashi K, Shinkura R, Koriyama C, Sakou T, et al: Pathogenesis of myelopathy in patients with ossification of the posterior longitudinal ligament. **J Neurosurg 96:**168–172, 2002
10. Matsunaga S, Sakou T, Taketomi E, Komiya S: Clinical course of patients with ossification of the posterior longitudinal ligament: a minimum 10-year cohort study. **J Neurosurg 100 (3 Suppl):**245–248, 2004
11. Matsuoka T, Yamaura I, Kurosa Y, Nakai O, Shindo S, Shinomiya K: Long-term results of the anterior floating method for cervical myelopathy caused by ossification of the posterior longitudinal ligament. **Spine 26:**241–248, 2001
12. Ogawa Y, Chiba K, Matsumoto M, Nakamura M, Takaishi H, Hirabayashi H, et al: Long-term results after expansive open-door laminoplasty for the segmental-type of ossification of the posterior longitudinal ligament of the cervical spine: a comparison with nonsegmental-type lesions. **J Neurosurg Spine 3:**198–204, 2005
13. Ono K, Ota H, Tada K, Hamada H, Takaoka K: Ossified posterior longitudinal ligament: a clinicopathological study. **Spine 2:**126–138, 1977
14. Tsuyama N: Ossification of the posterior longitudinal ligament of the spine. **Clin Orthop Relat Res 184:**71–84, 1984

Manuscript submitted August 2, 2008.
Accepted October 31, 2008.

Address correspondence to: Masashi Yamazaki, M.D., Ph.D., Spine Section, Department of Orthopaedic Surgery, Chiba University Graduate School of Medicine, 1-8-1 Inohana, Chuo-ku, Chiba 260-8677, Japan. email: masashiy@faculty.chiba-u.jp.

Acta Neurochir (Wien) (2008) 150: 575–582
DOI 10.1007/s00701-008-1574-1
Printed in The Netherlands

Acta Neurochirurgica

Technical Note

Anterior pedicle screw fixation for multilevel cervical corpectomy and spinal fusion

M. Aramomi, Y. Masaki, S. Koshizuka, R. Kadota, A. Okawa, M. Koda, M. Yamazaki

Spine Section, Department of Orthopaedic Surgery, Chiba University Graduate School of Medicine, Chuo-ku, Chiba, Japan

Received 12 September 2007; Accepted 1 March 2008; Published online 25 April 2008

Summary

Background. Prevention of graft dislodgement in multilevel cervical corpectomy and fusion has been an unresolved problem. Anterior plate fixation has a significant failure rate. External support with a halo-vest is uncomfortable for patients. In the present study, we report a new surgical technique of anterior pedicle screw (APS) fixation for multilevel cervical corpectomy and spinal fusion, and describe the safety and utility of the system.

Method. After cervical corpectomy, the pedicles on the right side were visualised under oblique fluoroscopy. Guide wires were inserted into the pedicles from the inner wall of the excavated vertebral body until they were hidden in the pedicles. After a fibula autograft was placed, the graft was penetrated in the reverse direction by the guide wires. After drilling and tapping, cannulated screws were inserted into the pedicles through the grafted fibula along the guide wires.

Findings. In 9 patients with cervical myelopathy, the surgery was accomplished with a fibula autograft using APS fixation. A total of 22 APSs were inserted, and 21 screws were placed precisely in the pedicles. There were no neurovascular complications. Patients were allowed to ambulate without a halo-vest on the second day after the surgery. Post-operatively, no dislodgement of the grated fibula occurred, and all patients improved neurologically.

Conclusions. The insertion of APSs is feasible and safe. APS fixation enables us to obtain rigid fixation anteriorly, and we propose that APS fixation is an attractive option for multilevel cervical corpectomy and fusion.

Keywords: Pedicle screw; anterior surgery; cervical spine; corpectomy; vertebral artery.

Introduction

Previous reports have shown that surgical outcomes of multilevel cervical corpectomy with spinal fusion are superior to those of laminoplasty in patients with cervical myelopathy, especially when the alignment of the cervical spine is kyphotic, and the spinal cord is severely compressed anteriorly [16, 20, 25, 26, 29].

Previous studies have shown that such problems as post-operative neck pain and stiffness, are less prominent after multilevel cervical corpectomy with spinal fusion when compared with those after laminoplasty [8, 15, 28].

Despite pre-operative information showing good surgical outcomes associated with anterior surgery, many patients (especially elderly patients) have selected posterior surgery [20]. The major reason for this selection is that the post-operative course of anterior surgery is often complicated. In particular, prevention of graft dislodgement in multilevel cervical corpectomy with spinal fusion has been an unresolved problem. Anterior plate fixation has a significant failure rate [5, 23, 27]. External

Correspondence: Masashi Yamazaki, MD, PhD, Spine Section, Department of Orthopaedic Surgery, Chiba University Graduate School of Medicine, 1-8-1 Inohana, Chuo-ku, Chiba 260-8677, Japan.
e-mail: masashiy@faculty.chiba-u.jp

support with a halo-vest decreases the dislodgement of the grafted bone, but application of the support is uncomfortable for patients [20]. Anterior and posterior plate fixation increases the stability of the constructs [6, 24], but requires a longer anaesthesia and is very laborious, including a change of the patient's surgical position.

We previously reported data showing the safety of anterior pedicle screw (APS) insertion in the cervical spine in an experimental study using cadavers (presented at the 19th annual meeting of the Cervical Spine Research Society-European Section, 2004). Based on those results, we began investigating the clinical application of APS fixation for multilevel cervical corpectomy with spinal fusion. In the present study, we describe the operative technique of APS fixation and report on its outcome.

Materials and methods

Patient population

From June 2004 to June 2006, 9 patients with cervical compression myelopathy underwent multilevel cervical corpectomy and spinal fusion with an autologous fibula graft using APSs (Table 1). The patients included 7 males and 2 females (average age at time of surgery = 56.3 years; range, 40–71 years). The average follow-up period was 16 months (range, 6–25 months). The cause of myelopathy were classified as ossification of the posterior longitudinal ligament (OPLL) in 4 patients, cervical spondylotic amyotrophy in 2, multilevel cervical disc herniation in 2, and cervical disc herniation accompanied by canal stenosis in the other patient. The fusion level was C3–C7 in 4 patients, C4–C7 in 3, C3–C6 in 1, and C5-T1 in 1.

Surgical technique of anterior pedicle screw fixation

As a representative example, we describe the surgical procedures for a patient (Number 3, Table 1), who underwent corpectomy of C5 and C6 and a fibula autograft fixed with APSs through the right C5 and C6 pedicles. The patient was placed in the supine position, and the patient's head was fixed with Mayfield's three pin system. With the patient in this position, we could obtain enough working space for surgery at the patient's nuchal area. Draping was performed so that the anterior and posterior aspects of the patient's neck were contained to the operative field.

Pre-operatively, we set the fluoroscopy angle at approximately 45° oblique to the floor and along the axis of the pedicles of C5 and C6. With such oblique fluoroscopy, we could detect the round-shaped cortex of the C5 and C6 pedicles on the right side of the cervical spine clearly.

A transverse collar incision of approximately 8 cm was made at the left side of the neck. The surgical approach extended along the esophagus and left carotid sheath, and the anterior aspect of the cervical vertebrae was exposed. After discectomy of C4/5, C5/6 and C6/7, cervical corpectomy of C5 and C6 was performed. Decompression of the spinal cord was confirmed by intraoperative spinal ultrasonography.

At the caudal aspect of C4 and the cranial aspect of C7, the endplate was removed by an air drill, and a graft bed for the strut fibula was prepared. The length required for the strut bone was measured. A piece of the left fibula was harvested from the patient's leg and prepared as a free strut graft to the site of corpectomy.

The right C6 pedicle was visualsed under oblique fluoroscopy. A guide wire, with both ends sharpened, was inserted into the pedicle from the inner wall of

Table 1. *Summary of data for 9 patients who underwent surgery with anterior pedicle screw fixation*

Case no.	Age (y)/ gender	Diagnosis	Fusion level	APS level	Follow-up period (mo)	JOA score		Solid graft union/period (mo)
						Before surgery	At follow-up	
1	44/M	OPLL	C4–C7	C5, C6	25	7.5	15	yes (12)
2	50/F	CDH&CS	C3–C6	C4, C5	24	12	16.5	yes (9)
3	64/M	CSAM	C4–C7	C5, C6	24	14.5	15.5	yes (14)
4	48/M	OPLL	C3–C7	C4, C5*, C6	18	1	7.5	yes (15)
5	40/M	MCDH	C4–C7	C5, C6	18	n.d.	n.d.	yes (12)
6	71/F	MCDH	C5–Th1	C6, C7	12	6	12	yes (12)
7	57/M	CSAM	C3–C7	C4, C5, C6	12	13	17	not yet
8	66/M	OPLL	C3–C7	C4, C5, C6	9	8	13.5	not yet
9	67/M	OPLL	C3–C7	C4, C5, C6	6	13	15	not yet

APS Anterior pedicle screw, *JOA* Japanese Orthopaedic Association, *OPLL* ossification of the posterior longitudinal ligament, *CDH&CS* cervical disc herniation and canal stenosis, *CSAM* cervical spondylotic amyotrophy, *MCDH* multilevel cervical disc herniation, *n.d.* not detected.

* The screw penetrated the lateral wall of the pedicle.

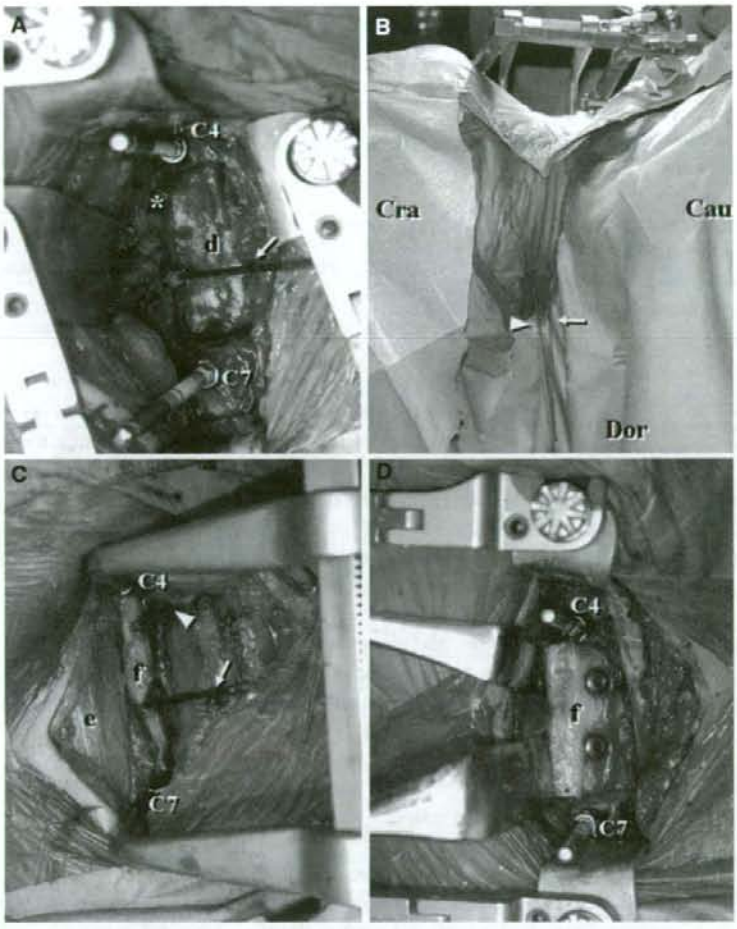

Fig. 1. Intra-operative photographs showing the process of anterior pedicle screw fixation for C5–C6 corpectomy and C4–C7 spinal fusion in a patient with cervical myelopathy (Patient 3). After corpectomy of C5 and C6, the right C6 pedicle was visualized under oblique fluoroscopy. (A) A guide wire (*arrow*) was inserted into the right C6 pedicle from the inner wall of the excavated vertebral body. The asterisk indicates the insertion point of the C5 pedicle screw. *d* Dura mater. (B) Guide wires were inserted deeply until they were hidden completely in the C5 and C6 pedicles. At this stage, the guide wires pass through the C5 pedicle (*arrowhead*) and the C6 pedicle (*arrow*) perforated the skin at the posterolateral area of the neck. The cranial side (*Cra*), caudal side (*Cau*) and dorsal side (*Dor*) of the patient are indicated. (C) After a fibula autograft (*f*) was placed, the graft was penetrated in the reverse direction by the guide wires through the C5 pedicle (*arrowhead*) and the C6 pedicle (*arrow*). *e* Esophagus. (D) After drilling and tapping, cannulated screws were inserted into the C5 and C6 pedicles through the grafted fibula (*f*) along the guide wires

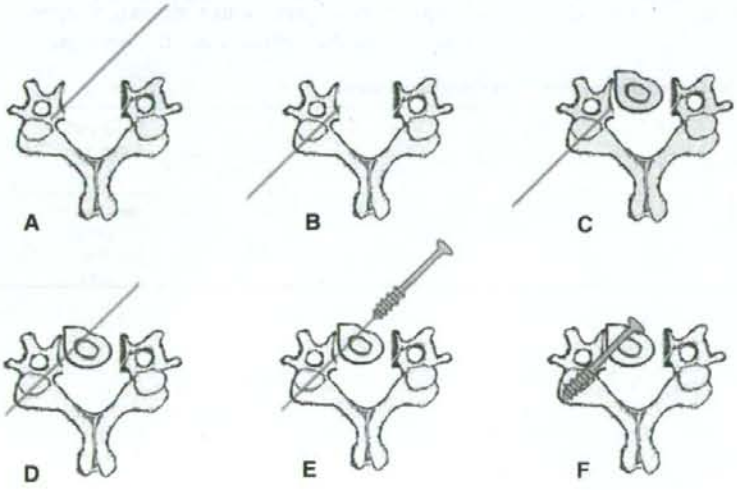

Fig. 2. Schematic drawings (A–F) showing the process of anterior pedicle screw fixation for multilevel cervical corpectomy and fusion

the excavated vertebral body under fluoroscopic guidance (Figs. 1A and 2A). It was inserted deeply, until it was hidden completely in the pedicle (Fig. 2B). At this stage, the guide wire perforated the skin at the posterolateral area of the neck (Fig. 1B). Another guide wire was placed similarly at the right C5 pedicle. The fibular autograft was tapped gently into place without interference by the guide wires (Fig. 2C). The graft was penetrated in the reverse direction by the guide wires (Figs. 1C and 2D). After drilling and tapping, a cannulated screw was inserted into the C6 pedicle through the graft along the guide wire (Fig. 2E, F). The length of the screw was determined pre-operatively by measuring the axial CT images. Similarly a screw was inserted at C5 (Fig. 1D).

On the second day after surgery, the patient was allowed to ambulate with a Philadelphia collar. At 6 weeks after surgery, a soft collar was used instead of the Philadelphia collar, and at 8 weeks after surgery, the soft collar was removed.

Clinical assessment

The Japanese Orthopaedic Association (JOA) scoring system was used to evaluate the severity of cervical myelopathy [20]. In 8 patients, the JOA scores before surgery and at the final follow-up after surgery were evaluated, and the recovery rate calculated. In patient 5, it was difficult to evaluate sensory and motor loss precisely, because the patient was mentally retarded.

Radiographic assessment

Accuracy of the insertion of the APSs was evaluated with CT reconstruction images. We determined that

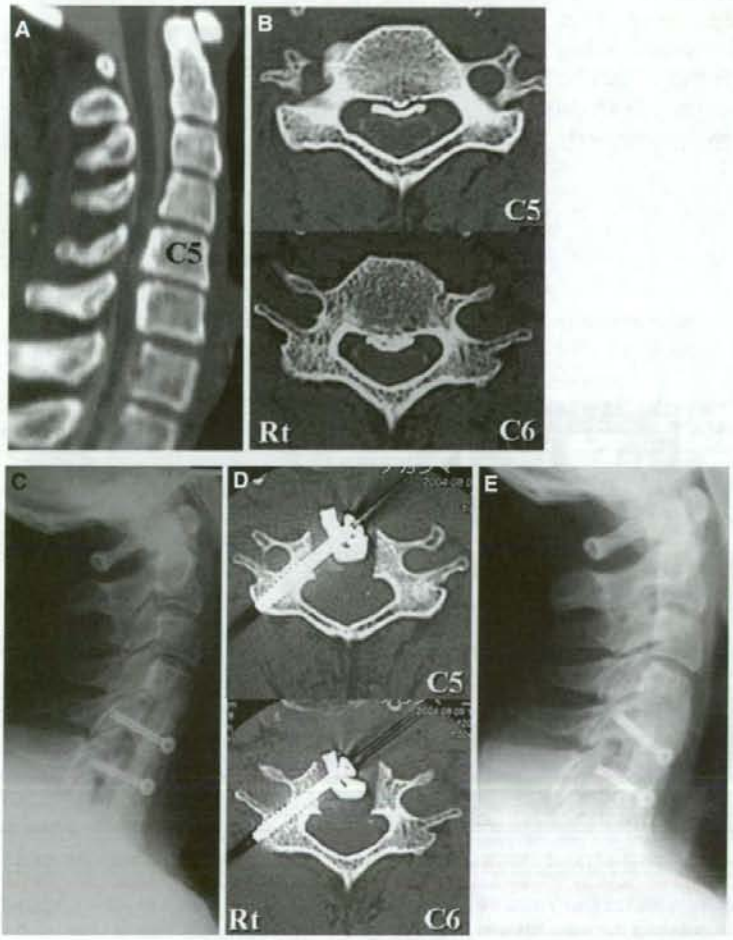

Fig. 3. Pre-operative midsagittal reconstruction image (A) and axial images at the C5 and C6 pedicles (B) of a CT myelogram of a 44-year-old man (Patient 1) showing OPLL at C4–C6 with compression of the spinal cord anteriorly at C5–C6. Post-operative lateral radiographic image (C) and axial views of CT (D) two weeks after surgery, indicating that the screws were inserted accurately through the grafted fibula autograft and the C5 and C6 pedicles. A lateral radiographic image two years after surgery (E), showing complete spinal fusion at C4–C7

the graft union was complete when intersegmental mobility within the fused segment was absent. A solid fusion was defined as ≤ 1 mm of change between flexion and extension radiographs in the interspinous distance across a grafted segment and by continuous osseous trabeculation at the site of the arthrodesis.

Results

A total of 22 APSs was inserted in this series. Among them, 21 screws were inserted precisely in the pedicles, and 1 screw perforated the lateral wall of the pedicle (C5 of patient 4). Thus, the pedicle perforation rate in this series was 4.5%. There were no neurovascular complications.

All 9 patients improved neurologically. The mean JOA score was 9.4 points before surgery and 14.0 points at the final follow-up, and the mean recovery rate was 64.4%.

There was no loosening or dislodgement of screws. No displacement of the grafted fibula occurred. Among 7 patients who were followed for more than 1 year after surgery, solid spinal fusion was detected in 6. The mean time to solid spinal fusion was 12.3 months (range, 9–15 months) after surgery.

Clinical presentations

Patient 1

A 44-year-old man presented with bilateral numbness in his upper and lower extremities and a spastic gait. The pre-operative JOA score was 7.5/17 points. Radiological examinations with CT myelogram and MR images showed C4–C6 OPLL associated with compression of the spinal cord anteriorly at C5–C6 (Fig. 3A, B).

At surgery, we first performed corpectomy of C5 and C6, extirpated the OPLL, and decompressed the spinal cord. We then harvested the fibula from his left leg and grafted it between C4 and C7. We inserted two APSs through the grafted fibula and the right C5 and C6 pedicles. Post-operative radiographs and CT images confirmed that the screws were inserted accurately through the pedicles (Fig. 3C, D), and no dislodgement of the grafted fibula was seen. At the final follow-up of 25 months, the patient's JOA score was 15/17 points (recovery rate: 79%), and complete spinal fusion was confirmed (Fig. 3E).

Patient 2

A 50-year-old woman presented with bilateral numbness and clumsiness in her hands. Her pre-operative JOA score was 12/17 points. Radiological examination with CT myelogram and MR images showed a central-type soft disc herniation at C4/5 and disc bulging at C5/6, which compressed the spinal cord anteriorly (Fig. 4A). She also had canal stenosis at the cervical spine; the anterior–posterior diameter of the spinal canal was 13 mm at C3, 12 mm at C4, 11.5 mm at C5, 13 mm at C6 and 13.5 mm at C7.

At operation, we first performed corpectomy of C4 and C5, extirpated the herniated discs, and decom-

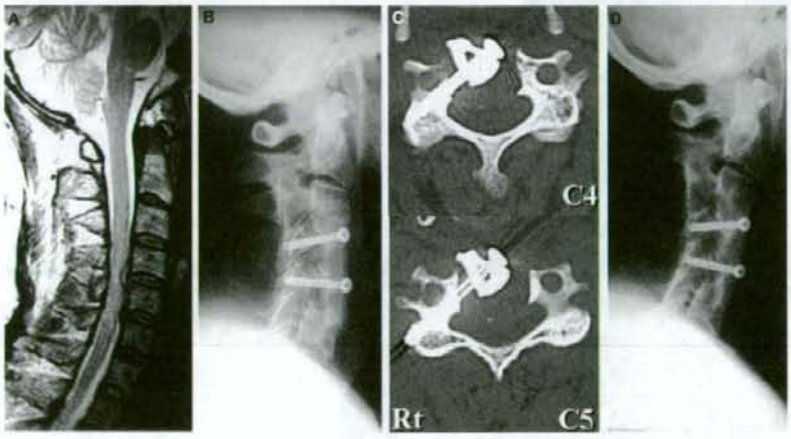

Fig. 4. Pre-operative T2-weighted MRI at the midsagittal plane (A) of a 50-year-old woman (patient 2) showing soft disc herniation at C4/5 and disc bulging at C5/6, which compressed the spinal cord anteriorly. Post-operative lateral radiographic image (B) and axial views of CT (C) two weeks after surgery, indicating that the screws were inserted accurately through the grafted fibula autograft and at the C4 and C5 pedicles. A lateral radiographic image two years after surgery (D), indicating that spinal fusion with the fibula autograft was complete at C3–C6

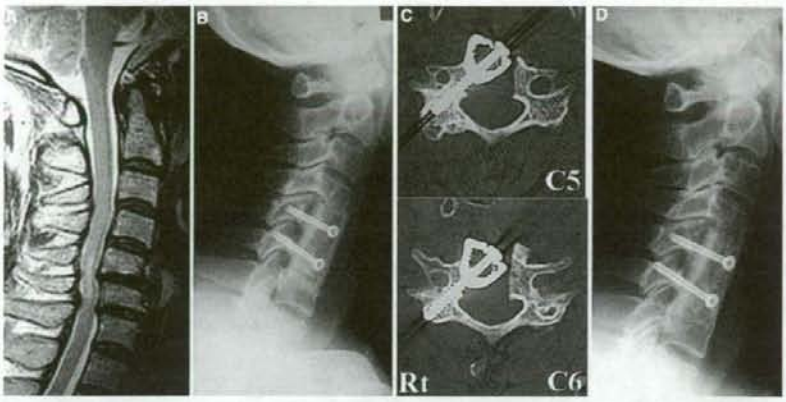

Fig. 5. Pre-operative T2-weighted MRI at the midsagittal plane (A) of a 64-year-old man (Case 3) showing osteophytes at C5/6 and C6/7, which compressed the spinal cord anteriorly. Post-operative lateral radiographic image (B) and axial views of CT (C) two weeks after surgery, indicating that the screws were inserted accurately through the grafted fibula autograft and the C5 and C6 pedicles. A lateral radiographic image two years after surgery (D), indicating that spinal fusion with the fibula autograft was complete at C4–C7

pressed the spinal cord. We then harvested the fibula from the left leg and grafted it between C3 and C6. We inserted two APSs through the grafted fibula and the right C4 and C5 pedicles. Post-operative radiographs and CT images confirmed that the screws were inserted accurately through the fibula autograft and the pedicles (Fig. 4B, C). At the final follow-up of 24 months, the patient's JOA score was 16.5/17 points (recovery rate: 90%), and complete spinal fusion was completed with an adequate alignment of the cervical spine (Fig. 4D).

Patient 3

A 64 year old man presented with muscle weakness and dysaesthesiae of his right upper extremity. His pre-operative JOA score was 14.5/17 points. Radiological examination with CT myelogram and MR images showed instability at C4/5 and osteophytes at C5/6 and C6/7, which compressed the spinal cord anteriorly (Fig. 5A).

At surgery, we first performed corpectomy of C5 and C6, extirpated the osteophytes and decompressed the spinal cord. We then harvested the fibula from his left leg and grafted it between C4 and C7. We inserted two APSs through the grafted fibula and the right C5 and C6 pedicles. Post-operative radiographs and CT images confirmed that the screws were inserted accurately through the pedicles (Fig. 5B, C). At the final follow-up of 24 months, the patient's JOA score was 15.5/17 points (recovery rate: 40%), and complete spinal fusion was confirmed without any dislodgement of the grafted fibula (Fig. 5D).

Discussion

Pedicle screws are useful tools for posterior fixation of the cervical spine [1–3]. The insertion of pedicle screws, however, has the potential risk of screw misplacement that causes damage to the spinal cord, nerve roots, or vertebral artery [4]. Previous studies have shown that the ratio of correct placement of ordinary posterior pedicle screws at the cervical spine ranges from 12.5 to 97% [4, 12–14, 18, 19, 21, 22]. Abumi *et al.* reported that the misplacement ratio of cervical posterior pedicle screws was 6.7% in their series (45 of 669 screws) [4]. Neo *et al.* inserted 86 pedicle screws in degenerative cervical vertebrae from the posterior direction, and 25 of them (29%) breached the pedicle walls [21].

In our APS fixation method, the vertebral artery is located at the lateral aspect of the entrance point, and the dura is directly visible in the surgical field. In addition, the ideal anterior entrance point of the APS can be identified using oblique fluoroscopy, which enables us to insert the APS into the pedicle accurately. When we compare the procedure for the placement of the APS with that of the posterior pedicle screw, the entrance point of the APS is closer to the pedicle (Fig. 6). Thus, the safety area at the insertion of the APS was larger than that of posterior pedicle screws. In fact, in the present series, 21 of 22 APSs were placed correctly in the pedicles, even though they were inserted into degenerative vertebrae. In this series, therefore, the misplacement ratio of APSs was 4.5%, which is principally lower than that of previously reported posterior pedicle screws [4, 21].

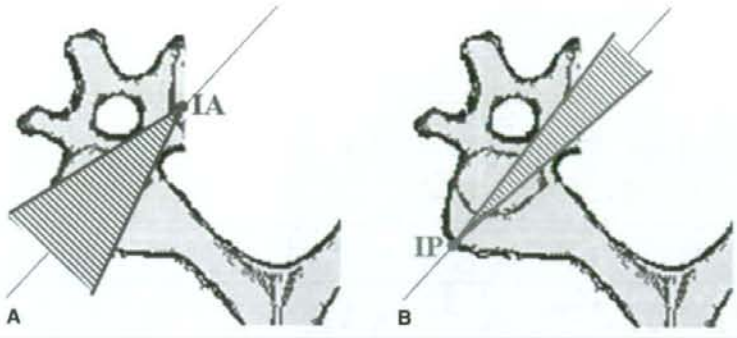

Fig. 6. Schematic drawings comparing the screw insertion points and the safety areas of the trajectory of an anterior pedicle screw (A) and a posterior pedicle screw (B). The safety area at the insertion of the anterior pedicle screw is larger than that of the posterior pedicle screw. The insertion points of the anterior (*IA*) and posterior (*IP*) pedicle screws are indicated

Fixation with an anterior plate and screws has several problems. The screws of the anterior construct are short and inserted monocortically to a vertebral body, which is sometimes made of fragile cancellous bone. Thus, anterior plating alone excessively loads the graft even with small degrees of motion, which may promote piston movement and failure of the anterior plate construct [7]. In particular, graft sinking is a major risk factor, which causes the failure of the anterior plate construct.

In contrast, fixation with APSs has several advantages. First, the pedicle is a strong anchor, even in osteoporotic patients [2]. Previous reports have proved biomechanical superiority of pedicle screws to conventional anterior and/or posterior cervical instrumentation methods [11, 17]. Another advantage is that the APS method does not fix the junction between the grafted bone and the vertebral body. This suggests that graft sinking does not reduce the stability of the construct.

Based on the considerations described above, we have begun clinical application of APS fixation. The present results showed that the insertion of APSs was safe, and no technical difficulty existed. Although a halo-vest was not applied post-operatively in this series, no dislodgement of the grafted fibula occurred. Graft sinking occurred to some extent during the follow-up period; however, bone union at the junction between the grafted fibula and the vertebral body progressed successfully. In this series, solid spinal fusion was detected 9–15 (mean 12.3) months after surgery. Previous reports showed that when multilevel cervical anterior fusion was performed with a fibular strut graft and post-operative halo-vest fixation, graft union was achieved at an average of 12 months after surgery [9, 10]. In the present series, the period for obtaining solid spinal fusion was almost the same as that in those previous reports. Thus, APS fixation can provide a rigid anterior fibula graft with minimum post-operative external support.

In conclusion, the present data demonstrates that insertion of APSs is feasible and safe. APS fixation could become a useful tool for obtaining rigid fixation of the grafted bone anteriorly when performing multilevel cervical corpectomy and spinal fusion.

References

1. Abumi K, Itoh H, Taneichi H, Kaneda K (1994) Transpedicular screw fixation for traumatic lesions of the middle and lower cervical spine: description of the techniques and preliminary report. J Spinal Disord 7: 19–28
2. Abumi K, Kaneda K (1997) Pedicle screw fixation for nontraumatic lesions of the cervical spine. Spine 22: 1853–1863
3. Abumi K, Kaneda K, Shono Y, Fujiya M (1999) One-stage posterior decompression and reconstruction of the cervical spine by using pedicle screw fixation systems. J Neurosurg 90: 19–26
4. Abumi K, Shono Y, Ito M, Taneichi H, Kotani Y, Kaneda K (2000) Complications of pedicle screw fixation in reconstructive surgery of the cervical spine. Spine 25: 962–969
5. Daubs MD (2005) Early failures following cervical corpectomy reconstruction with titanium mesh cages and anterior plating. Spine 30: 1402–1406
6. Epstein NE (2000) The value of anterior cervical plating in preventing vertebral fracture and graft extrusion after multilevel anterior cervical corpectomy with posterior wiring and fusion: indications, results, and complications. J Spinal Disord 13: 9–12
7. Foley KT, DiAngelo DJ, Rampersaud YR, Vossel KA, Jansen TH (1999) The *in vitro* effects of instrumentation on multilevel cervical strut-graft mechanics. Spine 30: 2366–2376
8. Hosono N, Yonenobu K, Ono K (1996) Neck and shoulder pain after laminoplasty: a noticeable complication. Spine 21: 1969–1973
9. Ikenaga M, Shikata J, Tanaka C (2005) Anterior corpectomy and fusion with fibular strut grafts for multilevel cervical myelopathy. J Neurosurg Spine 3: 79–85
10. Ikenaga M, Shikata J, Tanaka C (2006) Long-term results over 10 years of anterior corpectomy and fusion for multilevel cervical myelopathy. Spine 31: 1568–1574

11. Jones EL, Heller JG, Silcox DH, Hutton WC (1997) Cervical pedicle screws versus lateral mass screws: anatomical feasibility and biomechanical comparison. Spine 22: 977–982
12. Kamimura M, Ebara S, Itoh H, Tateiwa Y, Kinoshita T, Takaoka K (2000) Cervical pedicle screw insertion: assessment of safety and accuracy with computer-assisted image guidance. J Spinal Disord 13: 218–224
13. Karaikovic EE, Yingsakmongkol W, Gaines RW (2001) Accuracy of cervical pedicle screw placement using the funnel technique. Spine 26: 2456–2462
14. Kast E, Mohr K, Richter HP, Borm W (2006) Complications of transpedicular screw fixation in the cervical spine. Eur Spine J 15: 327–334
15. Kawaguchi Y, Matsui H, Ishihara H, Gejo R, Yoshino O (1999) Axial symptoms after en bloc laminoplasty. J Spinal Disord 12: 392–395
16. Kimura I, Shingu H, Nasu Y (1995) Long-term follow-up of cervical spondylotic myelopathy treated by canal-expansive laminoplasty. J Bone Joint Surg 77-B: 956–961
17. Kotani Y, Cunningham BW, Abumi K, McAfee PC (1994) Biomechanical analysis of cervical stabilisation systems: an assessment of transpedicular screw fixation in the cervical spine. Spine 19: 2529–2539
18. Ludwig SC, Kramer DL, Balderston, Vaccaro AR, Foley KF, Albert TJ (2000) Placement of pedicle screws in the human cadaveric cervical spine comparative accuracy of three techniques. Spine 25: 1655–1667
19. Ludwig SC, Kowalski JM, Edwards CC, Heller JG (2000) Cervical pedicle screws comparative accuracy of two insertion techniques. Spine 25: 2675–2681
20. Masaki Y, Yamazaki M, Okawa A, Aramomi M, Hashimoto M, Koda M, Mochizuki M, Moriya H (2007) An analysis of factors causing poor surgical outcome in patients with cervical myelopathy due to ossification of the posterior longitudinal ligament: anterior decompression with spinal fusion versus laminoplasty. J Spinal Disord 20: 7–13
21. Neo M, Sakamoto T, Fujibayashi S, Nakamura T (2005) The clinical risk of vertebral artery injury from cervical pedicle screws inserted in degenerative vertebrae. Spine 30: 2800–2805
22. Richter M, Cakir B, Schmidt R (2005) Cervical pedicle screws: conventional versus computer-assisted placement of cannulated screws. Spine 30: 2280–2287
23. Sasso RC, Ruggiero RA, Reilly TM, Hall PV (2003) Early reconstruction failures after multilevel cervical corpectomy. Spine 28: 140–142
24. Singh K, Vaccaro AR, Kim J, Lorenz EP, Lim TH, An HS (2003) Biomechanical comparison of cervical spine reconstructive techniques after a multilevel corpectomy of the cervical spine. Spine 28: 2352–2358
25. Suda K, Abumi K, Ito M, Shono Y, Kaneda K, Fujiya M (2003) Local kyphosis reduces surgical outcomes of expansive open-door laminoplasty for cervical spondylotic myelopathy. Spine 28: 1258–1262
26. Tani T, Ushida T, Ishida K, Iai H, Noguchi T, Yamamoto H (2002) Relative safety of anterior microsurgical decompression versus laminoplasty for cervical myelopathy with a massive ossified posterior longitudinal ligament. Spine 27: 2491–2498
27. Vaccaro AR, Falatyn SP, Scuderi GJ, Eismont FJ, McGuire RA, Singh K, Garfin SR (1998) Early failure of long segment anterior cervical plate fixation. J Spinal Disord 11: 410–415
28. Wada E, Suzuki S, Kanazawa A, Matsuoka T, Miyamoto S, Yonenobu K (2001) Subtotal corpectomy versus laminoplasty for multilevel cervical spondylotic myelopathy: a long-term follow-up study over 10 years. Spine 26: 1443–1447
29. Yamazaki A, Homma T, Uchiyama S, Katsumi Y, Okumura H (1999) Morphologic limitations of posterior decompression by midsagittal splitting method for myelopathy caused by ossification of the posterior longitudinal ligament in the cervical spine. Spine 24: 32–33

Comment

Aramomi *et al.* have analyzed a small series of patients who underwent anterior pedicle screw fixation for multilevel cervical corpectomy and spinal fusion. The anterior insertion of screws into the pedicles has been introduced as feasible and safe. The new anterior surgical approach was expected to increase stability and lower the risk of failures by using conventional anterior fixation methods. Even though the outcome in this small series was quite good, long-term results of much larger series will have to confirm this assumption. Nevertheless, this technical note is a nice introduction into a new fixation method performed from anteriorly. We agree that Halo-vests are very uncomfortable for patients who underwent cervical corpectomies and should be used only in special cases with significant morbidity. In fact, even Philadelphia collars can be avoided in most cases and a soft collar should be sufficient, provided intraoperative stability and screw firmness are confirmed. Although we would prefer iliac bone grafts instead of fibular grafts, this certainly would not change the overall idea of this paper. We are looking forward to see the reports of larger series from other groups using this elegant anterior fixation method.

Oliver Bozinov and *Helmut Bertalanffy*
Zurich, Switzerland

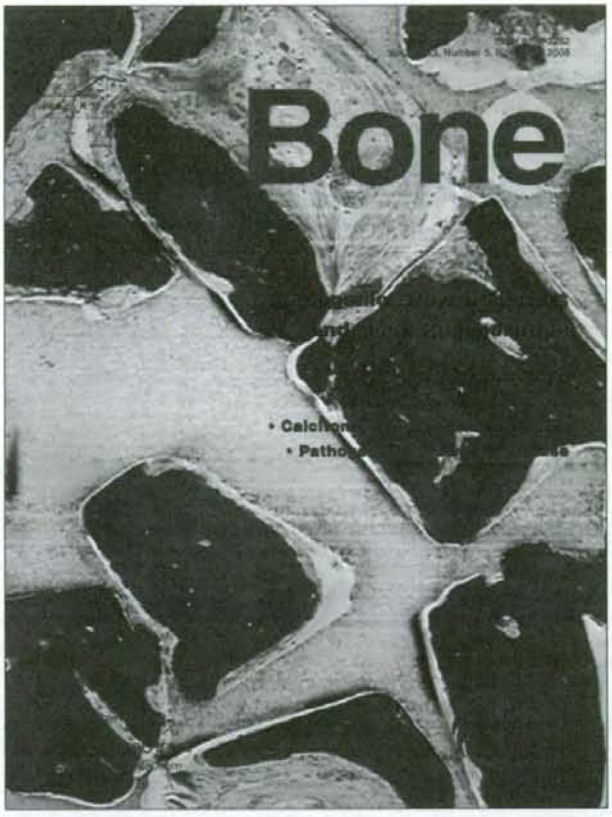

Bone 43 (2008) 832–839

Contents lists available at ScienceDirect

Bone

journal homepage: www.elsevier.com/locate/bone

Molecular basis for affected cartilage formation and bone union in fracture healing of the streptozotocin-induced diabetic rat

Akira Ogasawara [1], Arata Nakajima [2], Fumitake Nakajima [3], Ken-ichiro Goto [4], Masashi Yamazaki *

Department of Orthopaedic Surgery, Chiba University Graduate School of Medicine, Chiba, Japan

ARTICLE INFO

Article history:
Received 25 May 2008
Revised 21 July 2008
Accepted 25 July 2008
Available online 7 August 2008

Edited by: Thomas Einhorn

Keywords:
Diabetes
Fracture healing
Cartilage
Bone union
Molecular basis

ABSTRACT

Most studies have focused on the association between diabetes mellitus (DM) and impaired osseous healing, but there is also evidence that diabetes impairs cartilage formation during fracture healing. To investigate the molecular mechanisms by which diabetes affects endochondral ossification, experiments were performed in a model of rat closed fracture healing complicated with diabetes. Diabetic rats were created by a single intravenous injection of streptozotocin (STZ), while controls were treated with vehicle alone. Fractures were made 2 weeks after STZ injection. Animals were killed at 4, 7, 10, 14, 21, 28 and 42 days following fracture, and samples were subject to radiographic, histological and molecular analyses. In the DM group, a significantly smaller cartilaginous callus was formed compared with controls throughout healing, with the cartilage area being reduced rapidly after day 14. When the bone union rate was evaluated radiographically on day 28, DM calluses exhibited a lower rate than controls. However, when evaluated on day 42, both groups showed an equivalent union rate. Cellular proliferation of chondroprogenitor cells and proliferating chondrocytes in soft calluses of the DM group was significantly reduced during early stages of healing (days 4 and 7), but no longer reduced thereafter. Moreover, expression levels of collagen type II, type X and osteopontin (OPN) were constantly low in the DM group. These results show the molecular basis for diminished cartilage formation and delayed union in fracture healing of the STZ-induced diabetic rats.

Introduction

The association between diabetes mellitus (DM) and impaired osseous healing has been documented in clinical and experimental settings. Several clinical series have noted that the healing time for diabetic patients is approximately twice as long as that of non-diabetic patients [1,2]. In addition, diabetic patients undergoing arthrodesis had a significantly increased incidence of delayed union, non-union and pseudoarthrosis [3–5]. Chemically-induced and spontaneously developed diabetic animal models have demonstrated impaired fracture healing. In the various models of fracture healing, diabetes has led to reduced biomechanical properties of healing bones, reduced proliferation in the early callus, and reduced collagen synthesis and content compared to non-diabetic control animals [6–13].

One of the best-characterized models to study the impact of diabetes on bone in rats and mice is the induction of type 1 diabetes by streptozotocin (STZ). Treatment with STZ stimulates a host response that leads to destruction of pancreatic β cells, hypoinsulinemia and hyperglycemia, with many features similar to type 1 diabetes in humans [14–16]. Studies using this animal model show that there is a significant decrease in BMD, BMC and serum osteocalcin levels in the STZ-induced diabetic animals [17,18]. Moreover, there is a 20% decrease in biomechanical strength in both femurs and tibias [18,19]. BB rats, which are spontaneously diabetic, show similar reductions in BMD, serum osteocalcin levels and mechanical properties [20,21]. Long bone fractures of spontaneously diabetic or STZ-induced diabetic animals exhibit smaller calluses with decreased bone formation, proliferation and differentiation of osteoblastic cells and a 2-fold reduction in mechanical strength compared to matched controls [6,8,22,23].

Although most of the studies have focused on bone, there is also evidence that diabetes impairs cartilage formation (chondrogenesis) during fracture healing through decreased chondrocyte differentiation and proliferation [6,13,22,23]. Chondrogenesis, an essential component of endochondral ossification in long bones, is a key component of fracture healing. Growth factors and cytokines that are produced by the inflammatory response to skeletal injury support

* Corresponding author. Department of Orthopaedic Surgery, Chiba University Graduate School of Medicine, 1-8-1 Inohana, Chuo-ku, Chiba 260-8670, Japan. Fax: +81 43 226 2116.
E-mail address: masashiy@faculty.chiba-u.jp (M. Yamazaki).
[1] Current address: Department of Orthopaedic Surgery, Chosei Hospital, Mobara, Japan.
[2] Current address: Department of Orthopaedic Surgery, Chiba Aoba Municipal Hospital, Chiba, Japan.
[3] Current address: Department of Orthopaedic Surgery, Chiba Rosai Hospital, Ichihara, Japan.
[4] Current address: Department of Orthopaedic Surgery, Shimoshizu National Hospital, Yotsukaido, Japan.

8756-3282/$ – see front matter © 2008 Elsevier Inc. All rights reserved.
doi:10.1016/j.bone.2008.07.246

chemotaxis of immature mesenchymal cells to the site of fracture and promote their differentiation into chondrocytes. A well-organized development and maturation process leads to the formation of mineralized cartilage, which is subsequently replaced by bone [24,25]. It is therefore conceivable that diabetes impairs fracture healing by affecting not only bone (intramembranous) formation, but also cartilage (endochondral) development. However, the molecular mechanisms by which diabetes affects endochondral ossification in fracture healing have not been fully determined.

In the present study, a closed femoral shaft fracture was created in STZ-induced diabetic rats. We then performed detailed histological and molecular analyses, focusing on the spatial and temporal expression of cartilage-related collagen and non-collagen genes, to determine the impact of diabetes on fracture healing, particularly on endochondral ossification at molecular levels.

Materials and methods

Animals and materials

Two-month-old male Sprague–Dawley rats (10–12 weeks old; 300–400 g) were divided into two groups (control, $n=64$; diabetic, $n=62$). As a model for impaired fracture-repairing ability, diabetic rats were created by a single intravenous injection of 40 mg/kg STZ (Roche Molecular Biochemicals, Indianapolis, IN) in 0.1 M citrate buffer (pH 4.9). Rats with blood glucose levels over 300 mg/dl at 1 week after injection were used for experiments [7,13], and fractures were made 2 weeks after STZ injection. During experiments, the blood glucose levels were checked twice a week, and animals were excluded from the study if the blood glucose levels were less than 300 mg/dl in two consecutive measurements.

On days 4, 7, 10, 14, 21 and 28 following surgery, eight rats from each group were killed and the samples harvested in preparation for molecular ($n=4$) and histological ($n=4$) analyses. Day 42 samples (control, $n=12$; diabetic, $n=11$) were used only for radiographic analysis.

Fracture model

A standard, closed, mid-diaphyseal fracture was produced in the right femur of each rat according to Dr. Einhorn's fracture model [26]. Following anesthesia, a Kirschner wire (1.1 mm in diameter) was introduced into the medullary canal of the right femur, and a mid-diaphyseal fracture was created with an apparatus composed of a blunt guillotine driven by a dropped weight. These experimental procedures were approved by the Animal Care and Use Committee of Chiba University, Japan.

Radiographic analysis

When animals were sacrificed, radiographs were taken 7, 14, 28 and 42 days after the fracture. To judge bone union, eleven to twelve calluses from the control and DM groups were evaluated radiographically on days 28 and 42 post-fracture. On radiographic evaluation, four cortices (two on the antero-posterior and two on the lateral radiograph) on each callus were evaluated by at least two different authors (all are Orthopaedic surgeons), and a fracture callus was defined as a bony union when three of four cortices were bridged.

Tissue preparation

Four rats from each group were killed by intracardiac infusion of 4% paraformaldehyde under sodium pentobarbital anesthesia on days 4, 7, 10, 14, 21 and 28 (total 24 rats from each group) after production of fractures. Fractured femurs were removed with the surrounding tissues and fixed with 4% paraformaldehyde in 0.1 M PBS (pH 7.4) at 4 °C for 24 h. Tissues were decalcified at room temperature with 20% EDTA, 0.05 M Tris–HCl (pH 7.4), bisected sagittally in the median plane, and embedded in paraffin. Six-micrometer mid-sagittal sections were mounted on silane-coated slides.

Measurement of cartilage area

To visualize cartilage matrices, sagittal sections were stained with toluidine blue (pH 4.1), and areas showing metachromasia were identified as cartilage. Each callus was photographed using a standard light microscope. The cartilage area showing metachromasia was analyzed using NIH image (http://rsb.info.nih.gov/nih-image/).

Analysis of cellular proliferation in the soft callus

The fracture callus can be histologically divided into 'soft' and 'hard' calluses. Soft calluses consist of fibrous and cartilage tissues which are formed by endochondral ossification, while hard calluses consist of bone tissues which are formed by intramembranous ossification.

Sections were immunostained with a monoclonal antibody against proliferating cell nuclear antigen (PCNA) (PC-10; DAKO Japan, Kyoto, Japan) to evaluate cell proliferation. Immunochemical staining was performed as previously described [24,25,27,28]. Signals were detected using diaminobenzidine (DAB) followed by counterstaining with methylgreen. Four regions in the soft callus including cartilage or non-cartilaginous tissues were analyzed in each specimen, and the number of PCNA-positive cells was counted on days 4, 7 and 14 after fracture. Then the ratio of PCNA-positive cells to total cells was calculated and expressed as a percentage. The measurements were performed at least three times for one location of each specimen, and the average measurement obtained was defined as the PCNA score [24,25,27–29].

Preparation of probes

The following cDNA clones were used as hybridization probes in this study: mouse pro-α1 (II) collagen (COL2A1) cDNA containing a 0.64-kb fragment, mouse pro-α1(X) collagen (COL10A1) cDNA containing a 0.60-kb fragment and mouse osteopontin (OPN) cDNA containing a 1.2-kb fragment (a gift from Dr. S. Nomura, Osaka University, Japan). Specificity of these probes was confirmed previously [24,25].

RNA extraction and Northern blot analysis

For RNA extraction, rats were killed as described above on days 4, 7, 14, 21 and 28 post-operatively (total 20 rats from each group) and the fractured femurs were harvested. Tissues were frozen immediately in liquid nitrogen and stored at −80 °C until RNA isolation was performed. Total cellular RNA was extracted and mixed from four calluses for each group at different time points using TRIzol (Gibco BRL, Rockville, MD) according to the manufacturer's instructions. Twenty micrograms of total RNA from each daily sample was subjected to 1% agarose gel electrophoresis and transferred to a nylon membrane (Hybond-XL; Amersham Pharmacia Biotech, Buckinghamshire, UK). cDNA probes were labeled with ^{32}P using a random priming method. Northern blot analysis was carried out as previously described [24,25,27,28]. The density of each band on the autoradiogram was estimated by an image analyzer (Image Gauge software, version 3.1; FUJIFILM, Tokyo, Japan).

In situ hybridization

To compare distribution of cells expressing OPN mRNA in the fracture callus between groups, sections were hybridized with probes for OPN. Digoxigenin (DIG)-11-uridine 5-triphosphate-labeled single

strand RNA probes (antisense and sense probes) for mouse OPN cDNA (1.2-kb) were prepared. *In situ* hybridization was carried out as previously described [24,25,27]. Sections were hybridized with the antisense probes at 50 °C for 16 h, and signals were detected using the DIG detection kit (Roche Molecular Biochemicals, Indianapolis, IN). After signal detection, sections were counterstained with methyl-green. Sense probes were used to exclude the possibility of non-specific signals.

Statistical analysis

Differences between groups were determined by Chi-square for independence test or ANOVA. Where differences existed in ANOVA, the Fisher-protected least significant difference test was used to determine significance. A value of $p<0.05$ was considered statistically significant.

Results

Radiographic findings

In the control group, periosteal callus formation became visible by day 7 after fracture (Fig. 1A). By day 14, bony callus size had increased and a large radiolucent area was observed between periosteal calluses (Fig. 1B, arrows). By day 28, both the callus size and the radiolucent area between periosteal calluses had decreased gradually (Fig. 1C). Formation of osseous bridging over the fracture site was completed by day 42 (Fig. 1D). In contrast, periosteal callus formation was hardly detected on day 7 in the DM group (Fig. 1E). On day 14, a bony callus became visible but both the callus size and the radiolucent area between periosteal calluses were significantly smaller than controls (Fig. 1F, arrows). Even after day 14, the bony callus size did not increase and a radiolucent area was evident on day 28 (Fig. 1G), suggesting that bone union was delayed in the DM group at this stage. However, osseous bridging was completed by day 42, similar to control fractures (Fig. 1H).

Finally, we evaluated bone union rate at two different time points of the remodeling phase. On day 28, the union rate for control and DM groups was 58% (7 of 12) and 18% (2 of 11), respectively, with a significant difference noted between groups. However, on day 42, it was 83% (10 of 12) and 82% (9 of 11), respectively and there were no significant differences (Table 1).

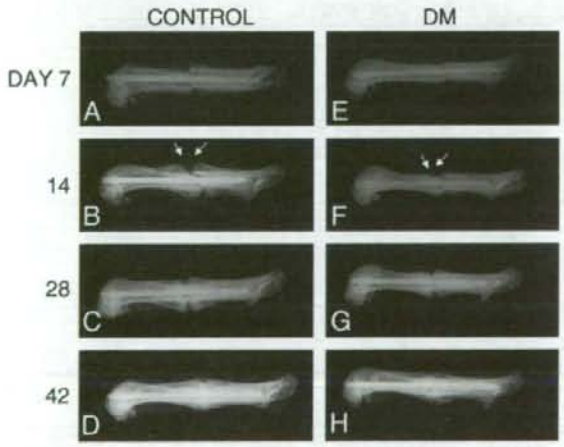

Fig. 1. Radiographic findings for the control (A–D) and the DM (E–H) callus during fracture healing. In the control group, a bony callus became evident by day 14 with a wide radiolucent area detected between periosteal calluses (B, arrows), while in the DM group, a smaller size of bony callus became visible on day 14 with a narrow radiolucent area detected (F, arrows). Note that the bony callus size of the DM group was smaller than that of controls during the entire healing period, but the final bone union (osseous bridging) was completed in both groups by day 42 (D, H).

Table 1
Bone union rates for the control and DM calluses

Union rate (%)	28 days	42 days
Control	7/12 (58%)	10/12 (83%)
DM	2/11 (18%)*	9/11 (82%)

* Significantly different from controls, $p<0.05$.

Morphological characteristics of cartilaginous areas in the fracture callus

The soft callus was divided into two distinct areas: non-cartilaginous granulation tissue and cartilage including spindle-

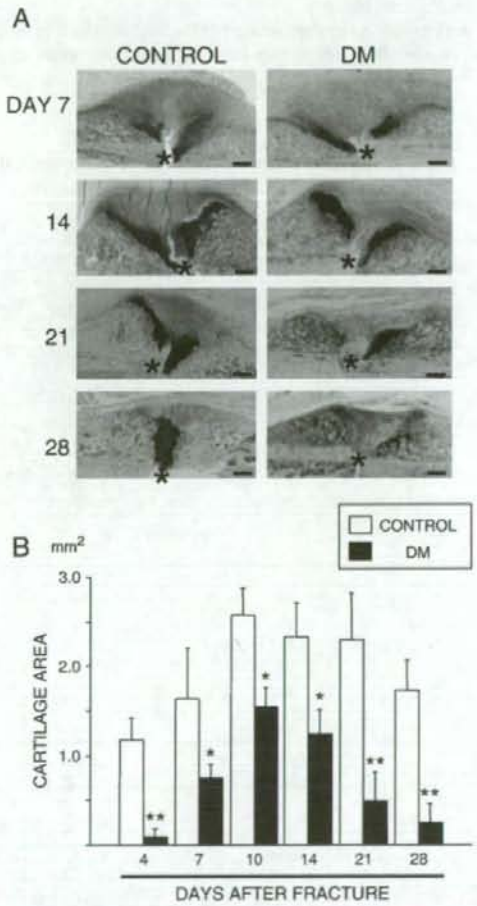

Fig. 2. (A) Histological features of the fracture callus for the control and DM groups. Mid-sagittal sections from the fracture callus on days 7, 14, 21 and 28 were stained with toluidine blue (pH 4.1). Areas showing metachromasia represent cartilage areas. Asterisks show the fracture site. Scale bars = 500 μm. (B) Changes in the cartilage area of the control and DM calluses during fracture healing ($n=4$ for each group at different time points). Note that in the DM group, a significantly smaller cartilage was developed and the cartilage area decreased rapidly after day 14, while in the control group, a moderate amount of cartilage still remained on day 28. The DM group exhibited a significant reduction in the cartilage area compared to controls at any time point up to day 28 following fracture. Each value represents a mean ± S.D. Values in which the DM group were significantly different from the matched control group (*$p<0.05$, **$p<0.01$).

shaped fibroblasts and round-shaped chondrocytes, respectively. In the soft callus of the control group, cartilage was clearly detected as a mass on day 7 after fracture and it was localized adjacent to the periosteal hard callus (Fig. 2A). Cartilage then expanded toward the center of the soft callus and its size increased until day 10. Thereafter, cartilage was replaced with trabecular bone and its size decreased gradually. On day 28, however, a moderate amount of cartilage remained between the hard calluses (Fig. 2B).

In the DM group, a significantly smaller cartilaginous callus was formed compared with controls throughout the entire healing period. On day 4, cartilage was hardly detectable. From day 7, a cartilage mass appeared and reached a maximum size on day 10, but the size was approximately 60% of control calluses. Reduction in the cartilage area then occurred and its size decreased rapidly up to day 28 (Fig. 2B).

Localization and quantification of PCNA-positive cells in the soft callus

Non-cartilaginous tissue

In both groups, granulation tissue at the fracture site was observed on day 4 after fracture. At this time point in the control group, a number of chondroprogenitor cells were stained with anti-PCNA antibodies (Fig. 3A-a). The PCNA score showed that 35% of cells in the granulation tissue were PCNA-positive (Fig. 3B). In the DM group, the number of chondroprogenitor cells showing PCNA immunoreactivity was significantly decreased (Fig. 3A-b) and only 12% of cells were PCNA-positive (Fig. 3B). On day 7, some of the chondroprogenitor cells around the cartilage mass were stained with anti-PCNA antibodies in both groups (data not shown). At this time point, the PCNA score of the DM group was 10%, while that of controls was 25%, with a significant difference between groups (Fig. 3B). By day 14, the number of PCNA-positive cells in non-cartilaginous tissue decreased rapidly in both groups. The PCNA score declined to around 10%, with no significant difference between groups (Fig. 3B).

Cartilage tissue

On day 7 after fracture, both groups showed small, round chondrocytes (proliferating chondrocytes) localized at the periphery of the cartilaginous mass, which were stained with anti-PCNA antibodies (Fig. 3A-c, d). At this time point, the PCNA score of the control and DM groups was 30% and 18%, respectively, with a

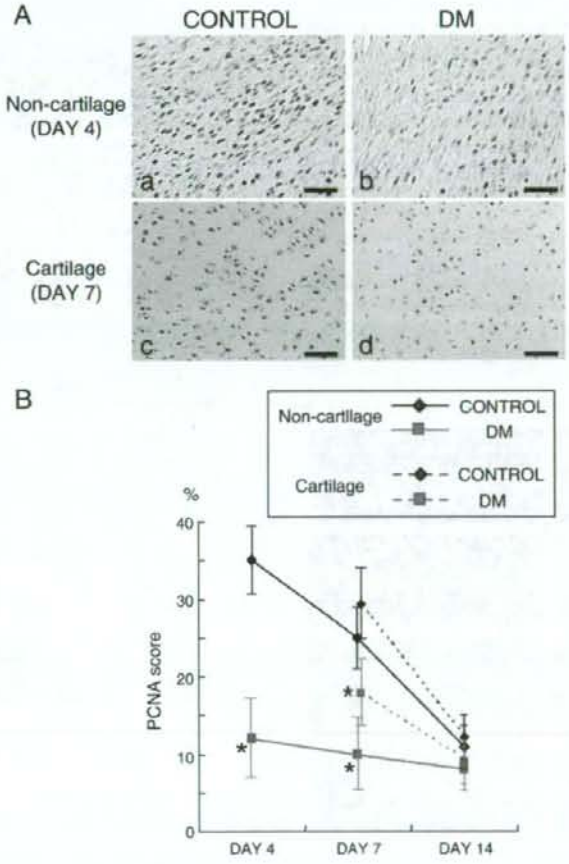

Fig. 3. (A) Cellular proliferation activity for non-cartilaginous and cartilage areas. The images show PCNA immunostaining for the control and DM groups on day 4 (a, b) and on day 7 (c, d) after fracture. In the DM group, the number of PCNA-positive chondroprogenitor cells in the non-cartilaginous area and proliferating chondrocytes in the cartilage area was significantly reduced compared to controls. Scale bars = 50 μm. (B) In the non-cartilaginous area, the PCNA score for the DM group (red square, solid line) was significantly reduced relative to controls (blue diamond, solid line) on days 4 and 7, but no longer reduced on day 14. In the cartilaginous area, the DM group (red square, dotted line) exhibited a significant reduction in the PCNA score compared to controls (blue diamond, dotted line) on day 7, but was not reduced on day 14. Each value represents a mean ± S.D. *Values in which the DM group were significantly different from the matched control group ($p < 0.05$).

significant difference noted between groups (Fig. 3B). On day 14, some of the proliferating chondrocytes were still PCNA-positive and hypertrophic chondrocytes were essentially negative in both groups (data not shown). The PCNA score for both groups declined to around 10% (Fig. 3B) with no significant difference between groups. On day 21, the score for both groups further decreased to less than 5% (data not shown).

Quantification of mRNA levels for cartilage-related collagen genes

mRNA expression of cartilage-related collagen genes, including COL2A1 and COL10A1, was examined at different time points in both groups and their levels were quantified (Figs. 4A, B). A considerable amount of COL2A1 was expressed in the control group on days 7 and 14. However, expression of COL2A1 mRNA was markedly reduced in the DM group (approximately 0.3-fold on days 7 and 14). Similarly, in both groups expression of COL10A1 appeared on day 7 and reached a maximum on day 14. From day 14 onwards, expression levels of COL10A1 for the DM group were lower than those for controls (approximately 0.6-fold on day 14 and 0.5-fold on day 21).

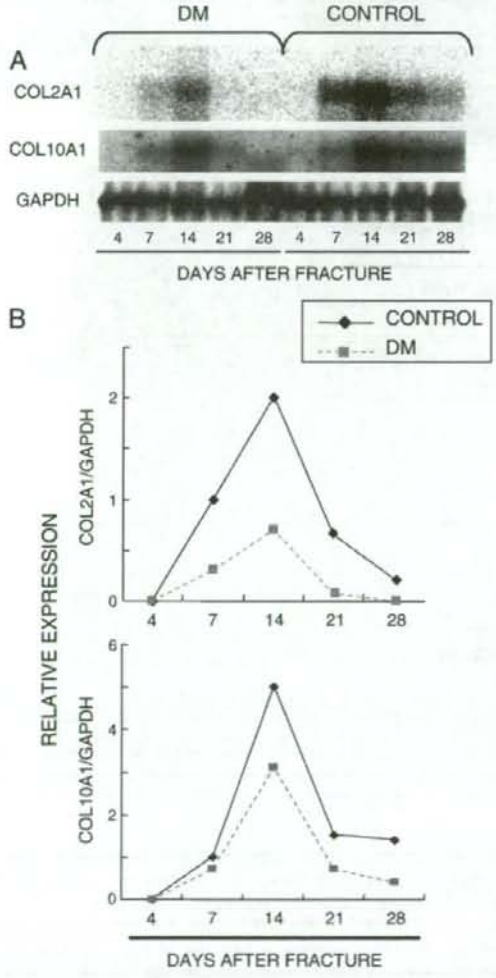

Fig. 4. (A) Northern blot analysis for the fracture callus of control and DM groups. Total cellular RNA was extracted and mixed from four calluses for each group at different time points. Twenty micrograms of total RNA from each daily sample was analyzed to quantify expression levels of cartilage-related genes, including COL2A1 and COL10A1. GAPDH served as an internal standard for the amount and integrity of RNA preparation. Representative autographic images are shown. (B) Quantification of mRNA expression levels for COL2A1 and COL10A1 in both groups. Each band density was normalized to the ratio of the internal standard GAPDH.

Analysis of spatial and temporal expression of OPN mRNA

Osteopontin (OPN) is one of the major non-collagenous extracellular matrix (ECM) proteins in bone. During endochondral ossification, OPN is expressed exclusively in late hypertrophic chondrocytes [30], and is thus a useful marker for terminal differentiation of chondrocytes. In the control group, a strong signal was detected in late hypertrophic chondrocytes that face osteoblasts in the primary spongiosa of the hard callus (Fig. 5A-a, red arrowheads). A weak to moderate signal was also observed in early hypertrophic chondrocytes (Fig. 5A-a). In the DM group, striking effects of diabetes on OPN expression were observed. Signal was hardly detected in late hypertrophic chondrocytes and no signal was seen in early hypertrophic chondrocytes, despite a moderate intensity of signal detected in osteoblasts in the primary spongiosa of the hard callus (Fig. 5A-b).

The temporal expression pattern for OPN mRNA was similar in both groups (Figs. 5B, C). There was a peak on day 14 when replacement of cartilage with bone was most prominent during healing. Expression levels of OPN for the DM group were reduced on days 7 and 14 (approximately 0.5-fold on day 7 and 0.6-fold on day 14). After day 14, the DM group exhibited a steady reduction in OPN expression, while the control group showed a sharp reduction from days 14 to 21 (Fig. 5C).

Discussion

Diabetes impairs the fracture healing process beginning with a reduction in early cellular proliferation, continuing with a delay in endochondral ossification and ending with a decrease in the biomechanical properties of the fracture callus [6–13,22]. In the present study, the molecular basis for impaired fracture healing was analyzed in the STZ-induced diabetic rat.

To examine the effect of diabetes on cartilage development during fracture healing, the cartilage area within the callus was measured. Both groups showed a peak on day 10, but the cartilage area of controls was 1.7-fold larger than that of the DM group. Interestingly, the DM group showed a sharp reduction in cartilage area after day 14. In contrast, the control group showed a steady reduction. This tendency was consistent with a previous study by Kayal et al. They demonstrated, using a tibial fracture model in mice, that callus size and cartilage area on day 12 were similar in normoglycemic and diabetic animals, but the DM group showed a sharp reduction in cartilage area from days 16 to 22, while the control group showed a steady reduction [32].

To elucidate the underlying mechanism by which a diabetic state led to a decrease in cartilage area, we first analyzed cellular proliferation in the soft callus, which consists of cartilage and non-cartilaginous tissues. The results showed that chondroprogenitor cells in the non-cartilaginous area of the DM group exhibited a significant decrease in cellular proliferation on days 4 and 7. Similar effects were observed in the cartilage area of the DM group on days 7 and 14. This is consistent with a previous study that showed a significant reduction of BrdU-positive cells during early stages of healing (on days 2 and 4) in the soft callus of a diabetic group compared to non-diabetic controls [6]. This decreased proliferation activity of chondrogenic cells in the DM group could also be supported by the fact that in fracture healing of insulin receptor substrate-1 (IRS-1)-deficient mice, where the signaling pathway of insulin and IGF-I is absent, the fracture site was associated with a decrease in chondrocyte proliferation [32].

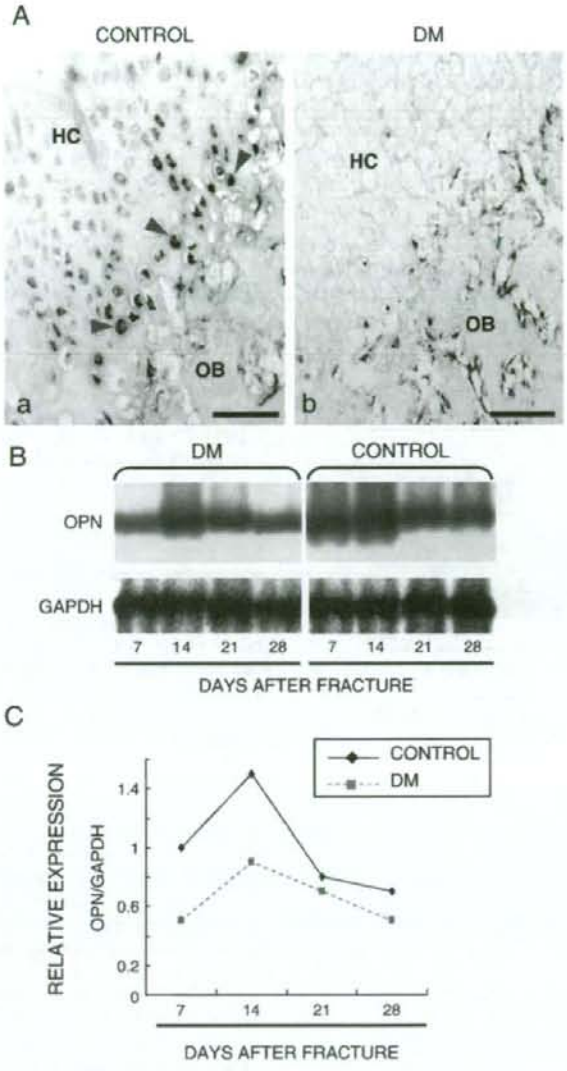

Fig. 5. (A) Spatial expression of OPN mRNA during the transition from cartilage to bone. Note that a strong signal was detected in late hypertrophic chondrocytes in the control group (a, red arrowheads). In contrast, a signal was hardly detected in the DM group (b). HC, hypertrophic chondrocytes; OB, osteoblasts. Scale bars = 50 μm. (B) Northern blot analysis for the fracture callus of control and DM groups. Total cellular RNA was extracted and mixed from four calluses for each group at different time points. Twenty micrograms of total RNA from each daily sample was analyzed to quantify expression levels of OPN. GAPDH served as an internal standard for the amount and integrity of RNA preparation. Representative autographic images are shown. (C) Quantification of mRNA expression levels for OPN in both groups. Each band density on B was normalized to the ratio of the internal standard GAPDH.

Next, we investigated anabolic activities of cartilage cells at the molecular level and mRNA expression of collagen type II (COL2A1) and type X (COL10A1) was quantified. Both groups showed a similar expression pattern, with a peak on day 14 and a sharp reduction thereafter. However, there was a constant reduction in expression for COL2A1 and COL10A1 in the DM group, suggesting that a diabetic state attenuates cartilage-related collagen synthesis from early to late stages of healing, leading to a smaller callus size.

It is currently controversial whether a diabetic state affects collagen expression during fracture healing. Gooch et al. reported that experimentally induced diabetic rats exhibited an alternation in the temporal expression of type II and type X collagen mRNA and a decrease in type X mRNA expression as compared to controls [23]. On the contrary, Kayal et al. showed that there was no significant difference in the expression of collagen I, II or X between diabetic and normal mice [31]. Differences could be explained by differing conditions of the experimental animals analyzed or when the samples were taken, but in the present study, a reduction in COL10A1 expression after day 14 was evident in the DM group. This led us to further investigate whether a diabetic state affects terminal differentiation of chondrocytes during endochondral ossification in fracture repair.

To this end, we focused specifically on the spatial and temporal expression of OPN, which is a well established marker for terminal differentiation of chondrocytes [25,33], and compared it between groups. The results showed that in the DM group, a signal was hardly detected in late hypertrophic chondrocytes in contrast to a robust

signal detected in controls. Quantitative data of OPN expression by Northern blot showed that the DM group expressed approximately 60% of the OPN levels of controls on day 14 and equivalent OPN levels during later stages (on days 21 and 28). Even though OPN is a useful marker for terminal differentiation of chondrocytes, osteoblasts also express a considerable amount of OPN, as shown in Fig. 5A. Thus, it is conceivable that total OPN expression in the DM group mostly reflects that derived from osteoblasts in the hard callus.

OPN plays important roles in a diverse set of processes including macrophage function, angiogenesis, extracellular matrix mineralization and osteoclastic bone remodeling, suggesting that OPN may be important during multiple stages of fracture healing. Of these OPN functions, osteoclastic resorption of mineralized cartilage is predominantly important during the transition from cartilage to bone. In this study, despite diminished expression of OPN, the cartilage area was reduced rapidly in the DM group, which was an unexpected result. Using OPN-deficient mice, Duvall et al. reported that OPN deficiency significantly altered, but did not prevent, bone regeneration and remodeling of fractures. Also, no compensatory over-expression of other ECM components was found [33]. These observations suggest that there may be redundant mechanisms that allow fracture healing to occur, albeit delayed, in the absence of OPN because of common cellular binding sites (e.g. RGD sequences) and functional overlap between OPN and other ECM proteins.

Another unexpected result in the present study was that there was no significant difference in the final bone union rate between groups evaluated on day 42. When the bone union rate was evaluated on day 28, the DM group exhibited a significantly lower rate than controls (Table 1). Nevertheless, both groups finally achieved an equivalent union rate, suggesting that a diabetic state delays but does not cease the endochondral ossification process in the middle of bone healing. However, due to the lack of mechanical testing, the equivalent union rate does not necessarily mean that quality of osseous healing is the same in the DM and control groups. We have previously shown that basic FGF-injected fracture calluses exhibited a lower bone union rate compared to controls due to enhanced cartilage formation [24,28]. Considering these observations, smaller cartilage development followed by enhanced cartilage removal in the DM callus may result in an equivalent final union rate as controls. However, a diabetic state definitely delayed the fracture healing process. Thus, insulin treatment or some type of intervention by bioactive agent(s) is indispensable to restore diabetes-induced impaired fracture healing to normal. Indeed, previous studies have demonstrated that systemic or local insulin treatment reversed impaired bone healing in diabetic animals, possibly through enhancement of bone formation and inhibition of bone resorption [6,8,11,34]. Of the bioactive agents other than insulin that enhance bone healing complicated with DM, parathyroid hormone (PTH) (1–34) may be a potent therapeutic agent because the effects of PTH (1–34) on bone and cartilage formation are thought to be largely insulin-like growth factor I-dependent [25,27].

In summary, the STZ-induced diabetic rats demonstrated impaired fracture healing associated with diminished chondrogenic cellular proliferation, cartilage-related collagen synthesis and delayed terminal differentiation of chondrocytes, which resulted in a smaller callus size. There were no significant differences in the final bone union rate between groups, although the mechanisms are still unclear. Future work will include examining molecular impacts of diabetes on later stages of fracture healing, in particular on cartilage and bone remodeling, and accelerating those stages by systemic or local treatment with insulin or some other bioactive agent(s).

Acknowledgments

We thank Dr Sumito Shimizu for his help to create the fractures of diabetic rats. This study was supported by a Grant-in-Aid for Scientific Research from the Ministry of Education, Science and Culture of Japan.

References

[1] Cozen L. Does diabetes delay fracture healing? Clin Orthop 1972;82:134–40.
[2] Loder RT. The influence of diabetes mellitus on the healing of closed fractures. Clin Orthop 1988;232:210–6.
[3] Papa J, Myerson M, Girard P. Salvage, with arthrodesis, in intractable diabetic neuropathic arthropathy of the foot and ankle. J Bone Joint Surg Am 1993;75: 1056–66.
[4] Stuart MJ, Morrey BF. Arthrodesis of the diabetic neuropathic ankle joint. Clin Orthop 1990;253:209–11.
[5] Tisdel CL, Marcus RE, Heiple KG. Triple arthrodesis for diabetic peritalar neuroarthropathy. Foot and Ankle Int 1995;16:332–8.
[6] Beam HA, Parsons JR, Lin SS. The effects of blood glucose control upon fracture healing in the BB Wistar rat with diabetes mellitus. J Orthop Res 2002;20: 1210–6.
[7] Funk JR, Hale JE, Carmines D, Gooch HL, Hurwitz SR. Biomechanical evaluation of early fracture healing in normal and diabetic rats. J Orthop Res 2000;18: 126–32.
[8] Herbsman H, Powers JC, Hirschman A, Shaftan GW. Retardation of fracture healing in experimental diabetes. J Surg Res 1968;8:424–31.
[9] Follak N, Kloting I, Wolf E, Merk H. Delayed remodeling in the early period of fracture healing in spontaneously diabetic BB/OK rats depending on the diabetic metabolic state. Histol Histopathol 2004;19:473–86.
[10] Follak N, Kloting I, Merk H. Influence of diabetic metabolic state on fracture healing in spontaneously diabetic rats. Diabetes Metab Res Rev 2005;21: 288–96.
[11] Macey LR, Kana SM, Jingushi S, Terek RM, Borretos J, Bolander ME. Defects of early fracture-healing in experimental diabetes. J Bone Joint Surg Am 1989;71: 722–33.
[12] Spanheimer RG. Correlation between decreased collagen production in diabetic animals and in cells exposed to diabetic serum: response to insulin. Matrix 1992;12:101–7.
[13] Topping RE, Bolander ME, Balian G. Type X collagen in fracture callus and the effects of experimental diabetes. Clin Orthop 1994;308:220–8.
[14] Herold K, Vezys V, Sun Q, Viktora D, Seung E, Reiner S, et al. Regulation of cytokine production during development of autoimmune diabetes induced with multiple low doses of streptozotocin. J Immunol 1996;156:3521–7.
[15] Sandberg J, Anderson A, Eizirik DA, Sandler S. Interleukin-1 receptor antagonist prevents low dose streptozotocin induced diabetes in mice. Biochem Biophys Res Commun 1994;202:543–8.
[16] Wang Z, Gleichmann H. GLUT2 in pancreatic islets: crucial target molecule in diabetes induced with multiple low doses of streptozotocin in mice. Diabetes 1998;47:50–6.
[17] Botolin S, Faugere MC, Malluche H, Orth M, Meyer R, McCabe LR. Increased bone adiposity and peroxisomal proliferator-activated receptor-gamma 2 expression in type I diabetic mice. Endocrinology 2005;146:3622–31.
[18] Hou J, Zernicke RF, Barnard R. Experimental diabetes, insulin treatment, and femoral neck morphology and biomechanics in rats. Clin Orthop 1991;264: 278–85.
[19] Reddy G, Stehno-Bittel L, Hamade S, Enwemeka C. The biomechanical integrity of bone in experimental diabetes. Diabetes Res Clin Pract 2001;54:1–8.
[20] Verhaeghe J, Suiker A, Nyomba B, Visser W, Einhorn T, Dequeker J, et al. Bone mineral homeostasis in spontaneously diabetic BB rats. II. Impaired bone turnover and decreased osteocalcin synthesis. Endocrinology 1989;124: 573–82.
[21] Verhaeghe J, van Herck E, Visser WJ, Suiker AM, Thomasset M, Einhorn TA, et al. Bone and mineral metabolism in BB rats with long-term diabetes. Decreased bone turnover and osteoporosis. Diabetes 1990;39:477–82.
[22] Gandhi A, Beam HA, O'Connor JP, Parsons JR, Lin SS. The effects of local insulin delivery on diabetic fracture healing. Bone 2005;37:482–90.
[23] Gooch HL, Hale JE, Fujioka H, Balian G, Hurwitz SR. Alternations of cartilage and collagen expression during fracture healing in experimental diabetes. Connect Tissue Res 2000;41:81–91.
[24] Nakajima F, Ogasawara A, Goto K, Moriya H, Ninomiya Y, Einhorn TA, et al. Spatial and temporal gene expression in chondrogenesis during fracture healing and the effects of basic fibroblast growth factor. J Orthop Res 2001;19: 935–44.
[25] Nakazawa T, Nakajima A, Shiomi K, Moriya H, Einhorn TA, Yamazaki M. Effects of low-dose, intermittent treatment with recombinant human parathyroid hormone (1–34) on chondrogenesis in a model of experimental fracture healing. Bone 2005;37:711–9.
[26] Bonnarens F, Einhorn TA. Production of a standard closed fracture in laboratory animal bone. J Orthop Res 1984;2:97–101.
[27] Nakajima A, Shimoji N, Shiomi K, Shimizu S, Moriya H, Einhorn TA, et al. Mechanisms for the enhancement of fracture healing in rats treated with intermittent low-dose human parathyroid hormone (1–34). J Bone Miner Res 2002;17:2038–47.
[28] Nakajima F, Nakajima A, Ogasawara A, Moriya H, Yamazaki M. Effects of a single percutaneous injection of basic fibroblast growth factor on the healing of a closed femoral shaft fracture in the rat. Calcif Tissue Int 2007;81:132–8.
[29] Iwaki A, Jingushi S, Oda Y, Izumi T, Shida J, Tsuneyoshi M, et al. Localization and quantification of proliferating cells during rat fracture repair: detection of proliferating cell nuclear antigen by immonohistochemistry. J Bone Miner Res 1997;12:96–102.
[30] Yamazaki M, Nakajima F, Ogasawara A, Moriya H, Majeska RJ, Einhorn TA. Spatial and temporal distribution of CD44 and osteopontin in fracture callus. J Bone Joint Surg Br 1999;81:508–15.